Journal of Applied Physics ARTICLE pubs.aip.org/aip/jap

Accurate heat flux formula and thermal conductivity calculation in molecular dynamics simulations with machine learning potentials

Cite as: J. Appl. Phys. **138**, 055105 (2025); doi: 10.1063/5.0278501
Submitted: 30 April 2025 · Accepted: 15 July 2025 ·
Published Online: 5 August 2025

Tomu Hamakawa,[1,2,3] Alan J. H. McGaughey,[2,a)] and Junichiro Shiomi[1,4,a)]

AFFILIATIONS

[1]Department of Mechanical Engineering, The University of Tokyo, Hongo, Bunkyo-Ku, Tokyo, Japan
[2]Department of Mechanical Engineering, Carnegie Mellon University, Pittsburgh, Pennsylvania 15213, USA
[3]The Institute of Statistical Mathematics, Research Organization of Information and Systems, Tachikawa, Tokyo, Japan
[4]Institute of Engineering Innovation, The University of Tokyo, Hongo, Bunkyo-Ku, Tokyo, Japan

[a)]**Authors to whom correspondence should be addressed:** mcgaughey@cmu.edu and shiomi@photon.t.u-tokyo.ac.jp

ABSTRACT

An accurate formula for the atomic heat flux that can be used in molecular dynamics (MD) simulations driven by machine learning potentials is derived and discussed. The equivalence of the Torii and Fan atomic heat flux formulas for any two- or many-body potential is first demonstrated. For copper and silicon modeled with three machine learning potentials [Spectral Neighbor Analysis Potential (SNAP), atomic cluster expansion potential, and moment tensor potential], the default heat flux formula implemented in the large-scale atomic/molecular massively parallel simulator is shown to over- or underestimate the lattice thermal conductivity compared with the accurate formula, with no systematic error based on the material or potential. The accuracy of the heat flux formula and its implementation are further demonstrated by comparing the temperature dependence of the lattice thermal conductivity of copper modeled with a SNAP potential with that obtained with anharmonic lattice dynamics calculations by solving the phonon Boltzmann transport equation incorporating up to four-phonon scattering. This study will facilitate accurate thermal conductivity calculations using MD simulations with machine learning potentials.

I. INTRODUCTION

Understanding and controlling heat conduction in solids is crucial for the thermal management of electronic devices and the development of thermoelectric materials.[1,2] Thermal conductivity indicates how efficiently heat is conducted in a material and is determined by its physical state and chemical composition. In insulating and semiconducting solids, heat is predominantly carried by atomic vibrations (i.e., phonons). Many computational studies have been conducted based on the theories of molecular dynamics (MD) and lattice dynamics (LD) to explore solid thermal conductivity.[3–8]

In a crystalline material, heat conduction can be described using the phonon-gas model (PGM), where the kinetics of phonon particles are solved using the Boltzmann transport equation (BTE) with phonon properties (modes, velocities, and scattering rates) obtained by LD calculations. Coupled with input from first-principles calculations, this approach has been successfully used to reproduce experimentally measured thermal conductivities for a range of materials.[5,7,9,10] LD approaches are based on perturbation theory and make assumptions related to small atomic displacements around the equilibrium lattice and how disorder is included.

MD simulations are a robust alternative to LD approaches in that they do not make any assumptions about the nature of the thermal transport. For example, they solve for atomic trajectories in real space without the need for a reference lattice and can naturally include any type of disorder. MD simulations have disadvantages in terms of the accuracy of the potential function and a lack of quantum statistics. The former has been significantly remedied by the development of machine learning potentials trained on first-principles data.[11–24] The latter needs to be considered when studying temperatures far below the material's Debye temperature.

There are two methods for calculating thermal conductivity using MD. These are based on non-equilibrium molecular dynamics (NEMD) and equilibrium molecular dynamics (EMD). The NEMD approach, commonly known as the direct method, applies high- and low-temperature regions to a simulation cell to generate a steady heat flux through the system.[25] The thermal conductivity can then be obtained using the Fourier law. By contrast, the EMD approach is based on the Green–Kubo method, which determines the thermal conductivity tensor κ through the heat flux autocorrelation function[26] from

$$\kappa = \frac{V}{k_B T^2} \int_0^\infty \langle \mathbf{J}(t) \otimes \mathbf{J}(0) \rangle \, dt, \tag{1}$$

where V is the volume, k_B is the Boltzmann constant, T is the temperature, $\mathbf{J}(t)$ is the atomic heat flux, and t is the time.

Irving and Kirkwood were the first researchers to derive a formula for the atomic heat flux.[27] Subsequently, Helfand derived a formula specific to two-body potentials,[28] which is referenced in the McQuarrie statistical mechanics textbook.[29] In applying Eq. (1), many researchers have cited Ref. 29 and used Helfand's formula for both two- and many-body potentials. There have been numerous reports, however, on how the heat flux should be formulated for many-body potentials. Hardy rigorously derived a many-body local heat flux formula from a local energy-conservation equation.[30] Torii *et al.* derived a formula for many-body potentials (Torii formula).[6,31] Surblys *et al.* derived the centroid formula as a specific version of the Torii formula, assuming the equipartition of interaction energies.[32,33] They compared their centroid formula with the approximate formula used in the Large-scale Atomic/Molecular Massively Parallel Simulator (LAMMPS),[34] which is a widely used MD simulation software package. The LAMMPS approximate formula assumes the equipartition of the virial contribution for each many-body interaction.[35] Surblys *et al.* computationally confirmed the accuracy of their centroid formula by comparing it with the Torii formula and showed that the default LAMMPS formula overestimated the thermal conductivity by up to 1.3 times for butane modeled with the NERD potential. They also implemented the centroid formula in LAMMPS. Boone *et al.*[36] further explored the discrepancies between the Torii and LAMMPS approximate formulas. Fan *et al.* derived a rigorous formula (Fan formula) based on Hardy's derivation and applied it to the three-body Tersoff potential.[37] They implemented their formulation in the Graphical Processing Unit Molecular Dynamics (GPUMD) package.[38]

Recently, the principle of the gauge invariance of the heat flux has been reported.[39–41] This invariance arises from the ambiguity in partitioning the total potential energy among individual atoms, allowing the heat flux to be transformed into an equivalent expression via a gauge transformation. While such a transformation can affect the convergence speed of the integration of the heat flux autocorrelation, it leaves the final converged value unchanged. If the original heat flux expression—particularly its virial term—however, is inherently incorrect, the resulting thermal conductivity will also be incorrect, regardless of the gauge transformation applied.

In recent years, machine learning potentials trained on first-principles data have attracted considerable attention.[11–24] Machine learning potentials are methods for predicting atomic energies and forces using machine learning models or the potentials created by such methods. Although machine learning potentials have the same level of accuracy as their training data, which are typically taken from density functional theory (DFT) calculations, they are much more computationally efficient to evaluate. As a result, there are an increasing number of reports on calculating the thermal conductivity of existing and new materials using machine learning potentials.[42–45] Machine learning potentials are generally classified as many-body potentials. It is, thus, essential to use an accurate heat flux formula when using the Green–Kubo EMD approach. Langer *et al.*[46] discussed the applicability of the Fan formula to machine learning potentials. They developed an efficient method to calculate the heat flux for message-passing neural network potentials.

The Torii and Fan formulas have been established as reliable expressions for calculating the heat flux in systems with many-body potentials.[6,37] The relationship between these two expressions, however, has not yet been clarified. Moreover, although recent work has reported that the Fan formula is applicable to machine learning potentials, the applicability of the Torii formula in this context remains uncertain.

In this study, we derive an accurate heat flux formula for machine learning potentials. In Sec. II, we outline the functional form of machine learning potentials. In Secs. III B and III C, we present the Torii and Fan formulas, the current de facto standards of the heat flux formula for many-body potentials. In Sec. III D, we demonstrate the applicability of these formulas to machine learning potentials and confirm their consistency. In Sec. IV, we examine the current LAMMPS implementation, highlighting differences compared to the accurate formula. Finally, we perform EMD simulations for Si and Cu to demonstrate the differences between the accurate and approximate formulas and then compare the thermal conductivities obtained using the Green–Kubo approach with those obtained using the BTE.

II. METHOD: MACHINE LEARNING POTENTIAL

A. General functional form of a machine learning potential

We first examine the general functional form of a machine learning potential. This step is critical for determining the precise formulation of the atomic energies necessary for the heat flux formula.

Both empirical and machine learning potentials have been developed to approximate *ab initio* energies from DFT calculations. The *ab initio* energy depends on the positions of all the atoms within the simulation. Although the atoms consist of electrons and nuclei, we define the atomic positions as the center of the nuclei. The *ab initio* energy can then be expressed as $E^{\mathrm{DFT}}(\mathbf{r}_1, \mathbf{r}_2, \ldots, \mathbf{r}_N)$, where $\{\mathbf{r}_1, \ldots, \mathbf{r}_N\}$ denotes the atomic positions and N is the number of atoms in the system. The application of a potential to an MD simulation should not depend on the number of atoms in the system. Machine learning potentials are, thus, designed to provide per-atom potential energies. Hence, we begin by decomposing the *ab initio* energy into the atomic energies ψ_i as

$$E^{\mathrm{DFT}}(\mathbf{r}_1, \mathbf{r}_2, \ldots, \mathbf{r}_N) \simeq \sum_{i=1}^{N} \psi_i(\mathbf{r}_1, \mathbf{r}_2, \ldots, \mathbf{r}_N). \tag{2}$$

Although we assume a simple, single element substance, the decomposition in Eq. (2) can be readily expanded to a multi-element system.[47] We then write the potential energy of atom i as a function of the relative position vectors with respect to that atom as[48]

$$\psi_i(\mathbf{r}_1, \mathbf{r}_2, \ldots, \mathbf{r}_N) = \tilde{\psi}_i(\mathbf{r}_1 - \mathbf{r}_i, \mathbf{r}_2 - \mathbf{r}_i, \ldots, \mathbf{r}_N - \mathbf{r}_i). \quad (3)$$

Here, we define the set of relative position vectors, $\{\mathbf{r}_1 - \mathbf{r}_i, \mathbf{r}_2 - \mathbf{r}_i, \ldots, \mathbf{r}_N - \mathbf{r}_i\}$ as the local chemical environment (LCE) $\mathfrak{n}_i$. In addition, we replace $\tilde{\psi}_i$ with the simplified notation ψ_i.

The LCE is an abstract quantity representing the chemical environment around a specific atom. The set of relative position vectors is one possible representation of the chemical environment. The LCE could also be expressed in terms of bond lengths and angles, and if the system is a multi-element system, it must include the types of elements. If the system contains only a single element type, then all chemical information is included in the relative position vectors without excess or deficiency because the inner product between relative vectors contains information about the bond angles. Therefore, we employ $\mathfrak{n}_i$ in this study. In addition, we define the vector $[x_1 - x_i, y_1 - y_i, z_1 - z_i, \ldots, z_N - z_i]^\top$ as $\mathbf{r}_{\mathfrak{n}_i} \in \mathbb{R}^{3N}$. When the simulation system is sufficiently large, the energy functions $\psi_1(\mathbf{r}_{\mathfrak{n}_1}), \ldots, \psi_N(\mathbf{r}_{\mathfrak{n}_N})$ have the same functional form, regardless of the atom index, such that

$$\psi_i(\mathbf{r}_{\mathfrak{n}_i}) = \psi(\mathbf{r}_{\mathfrak{n}_i}). \quad (4)$$

The *ab initio* energy can, thus, be expressed as

$$E^{\mathrm{DFT}}(\mathbf{r}_1, \mathbf{r}_2, \ldots, \mathbf{r}_N) = \sum_{i=1}^{N} \psi(\mathbf{r}_{\mathfrak{n}_i}). \quad (5)$$

The approximations leading to Eq. (5) are applied not only when using machine learning potentials but also when using empirical potentials. A low computational cost is generally required for training potentials. To address this need, symmetry can be incorporated into the input as *a priori* knowledge of the material. This idea is equivalent to choosing an input that is theoretically or empirically related to the output of a machine learning model. For input to a machine learning potential, the relative position vectors $\mathbf{r}_{\mathfrak{n}_i}$ are converted to another representation that includes known symmetries,

$$\begin{aligned} \phi &: \mathbb{R}^{3N} \to \mathbb{R}^m, \\ \phi_i &= \phi(\mathbf{r}_{\mathfrak{n}_i}). \end{aligned} \quad (6)$$

Here, the mapping ϕ has symmetry with respect to the rotation operator $\hat{R}(\theta)$ such that

$$\phi(\mathbf{r}_{\mathfrak{n}_i}) = \phi(\hat{R}(\theta)\mathbf{r}_{\mathfrak{n}_i}). \quad (7)$$

Equivariance with respect to the rotational operation[24] is recently used instead of the invariance in Eq. (7). The potential energy must also remain constant across all permutations of the atoms. The mapping ϕ, thus, also has the following symmetry with respect to the permutation operator $\hat{\sigma}$:

$$\phi(\mathbf{r}_{\mathfrak{n}_i}) = \phi(\hat{\sigma}\mathbf{r}_{\mathfrak{n}_i}). \quad (8)$$

The function ϕ is also known as a descriptor, which is the input for predicting the atomic energies. To enhance the prediction accuracy with less training data, other LCE representations have been developed.[49]

If we write the machine learning model as f^{ML}, the machine learning potential is described by the composite function $f^{\mathrm{ML}} \circ \phi$, which uses the relative position vectors $\mathbf{r}_{\mathfrak{n}_i}$ as input, i.e.,

$$\begin{aligned} f^{\mathrm{ML}} &: \mathbb{R}^m \to \mathbb{R}, \\ \psi_i &\simeq f^{\mathrm{ML}}(\phi_i) = f^{\mathrm{ML}}(\phi(\mathbf{r}_{\mathfrak{n}_i})) = f^{\mathrm{ML}} \circ \phi(\mathbf{r}_{\mathfrak{n}_i}). \end{aligned} \quad (9)$$

The development of machine learning potentials can be, thus, categorized into two primary areas: the development of the function ϕ and the design of the machine learning model f^{ML}.

B. Example: Moment tensor potential

We now consider the moment tensor potential (MTP)[18] as an example of a machine learning potential that is characterized by intricate descriptors. The MTP uses moment tensors $M_{\mu,\nu}$ for constructing the descriptors,[18,19,50,51]

$$M_{\mu,\nu}(\mathbf{r}_{\mathfrak{n}_i}) = \sum_j f_\mu(r_{ij}, z_i, z_j)\mathbf{r}_{ij}^{\otimes\nu}. \quad (10)$$

Here, the f_μ are polynomial functions, z_i and z_j are the element types of the atoms i and j, and the tensor $\mathbf{r}_{ij}^{\otimes\nu}$ is the tensor product of the vector $\mathbf{r}_{ij}$ multiplied by itself ν times. The descriptor $\{B\}$ is composed of scalars obtained from moment tensors. The machine learning model employs linear regression, with the atomic potential energy expressed as

$$\psi_i = \sum_{k=1}^{|\{B\}|} c_k B_k(\mathbf{r}_{\mathfrak{n}_i}). \quad (11)$$

Here, c_k are the trainable parameters. By expressing this function as shown in Eq. (9), the descriptor and machine learning model are

$$\phi(\mathbf{r}_{\mathfrak{n}_i}) = [B_1(\mathbf{r}_{\mathfrak{n}_i}), B_2(\mathbf{r}_{\mathfrak{n}_i}), \ldots]^\top, \quad (12)$$

$$f^{\mathrm{ML}}(\phi) = \sum_k c_k \phi_k. \quad (13)$$

Usually, $B_1(\mathbf{r}_{\mathfrak{n}_i})$ is $M_{0,0}(\mathbf{r}_{\mathfrak{n}_i})$, $B_2(\mathbf{r}_{\mathfrak{n}_i})$ is $M_{0,0}^2(\mathbf{r}_{\mathfrak{n}_i})$, and $B_3(\mathbf{r}_{\mathfrak{n}_i})$ is $M_{0,1}(\mathbf{r}_{\mathfrak{n}_i}) \cdot M_{0,1}(\mathbf{r}_{\mathfrak{n}_i})$.

III. HEAT FLUX FORMULA FOR MACHINE LEARNING POTENTIALS

A. Heat flux formula for many-body potential

The Torii formula[6,31–33] and Fan formula[37] are the current de facto standards for the heat flux formulation of many-body potentials. The Torii formula is introduced in Sec. III B. As no studies to date have shown the applicability of the Torii formula to machine learning potentials, it is derived in detail. Subsequently, in Sec. III C, we briefly present the Fan formula, which is known to be applicable to machine learning potentials.[46] Finally, in Sec. III D, we demonstrate that the Torii formula is equivalent to the Fan formula not only for machine learning potentials but also for empirical potentials.

For simplicity, we considered a simple, single element substance. The heat flux can be calculated using the time derivative of the Helfand moment,[28]

$$V\mathbf{J} = \frac{d}{dt}\sum_{i=1}^{N}(\varepsilon_i - \langle\varepsilon_i\rangle)\mathbf{r}_i = \sum_{i=1}^{N}(\varepsilon_i - \langle\varepsilon_i\rangle)\mathbf{v}_i + \sum_{i=1}^{N}\frac{d\varepsilon_i}{dt}\mathbf{r}_i. \tag{14}$$

Here, ε_i is the total energy (potential and kinetic) of atom i and $\mathbf{v}_i$ is the velocity of atom i. The first term is called the convective term and the second term is called the virial term. In the remainder of this study, we ignore the convective term because its formulation is unambiguous.

B. Torii formula

Let the many-body interactions be up to m-body, and let ϕ_n be the potential energy function for the n-body interaction. The set of these potential functions is defined as $\mathscr{V} = \{\phi_1, \ldots, \phi_m\}$. For each potential function, denote an n-body atomic cluster as U_n^j, and a set of n-body clusters as $\mathbf{U}_n = \{U_n^1, \ldots\}$. For example, in the case of a two-body interaction, the set of atomic pairs is represented by $\mathbf{U}_2 = \{(1,2), \ldots, (N-1, N)\}$. Thus, the potential energy of atom i is expressed as

$$\psi_i = \sum_{\phi_n\in\mathscr{V}}\sum_{U_n^{(i)}\in\mathbf{U}_n} p_{i,U_n^{(i)}}\phi_n\left(\mathbf{r}_i, \mathbf{r}_{s_1}, \ldots, \mathbf{r}_{s_{n-1}} \middle| i, s_1, \ldots, s_{n-1} \in U_n^{(i)}\right). \tag{15}$$

In Eq. (15), $U_n^{(i)}$ is the n-body cluster that includes the atom i, s_j is the index of atoms within $U_n^{(i)}$, and $\sum_{U_n^{(i)}\in\mathbf{U}_n}$ represents the summation over all such clusters $U_n^{(i)}$. The contribution ratio $p_{i,U_n^{(i)}}$ is the fraction of the potential energy $\phi_n\left(U_n^{(i)}\right) := \phi_n\left(\mathbf{r}_i, \mathbf{r}_{s_1}, \ldots, \mathbf{r}_{s_{n-1}} \middle| i, s_1, \ldots, s_{n-1} \in U_n^{(i)}\right)$ that is assigned to the atom i. For example, considering the two-body Lennard–Jones potential, the interaction energy $\mathrm{LJ}(r_{ij})$ between atoms i and j is generally distributed equally between them. Therefore, the potential energy of atom i is written as

$$\psi_i = \sum_{j=1, j\neq i}^{N}\frac{1}{2}\mathrm{LJ}(r_{ij}). \tag{16}$$

The contribution ratio p is 1/2 for all the pairs in the LJ system. Generally, the contribution ratio p_{j,U_n} must satisfy

$$\sum_{j\in U_n} p_{j,U_n} = 1. \tag{17}$$

Because the atomic energy consists of potential energy and kinetic energy, the time derivative of the atomic energy is written as

$$\frac{d\varepsilon_i}{dt} = \frac{d}{dt}\left(\frac{1}{2}m_i\mathbf{v}_i^2 + \psi_i\right) = \left\{\mathbf{v}_i\cdot\mathbf{F}_i + \sum_{\phi_n\in\mathscr{V}}\sum_{U_n^{(i)}\in\mathbf{U}_n} p_{i,U_n^{(i)}}\frac{d}{dt}\phi_n\left(U_n^{(i)}\right)\right\}, \tag{18}$$

where m_i is the mass of atom i and $\mathbf{F}_i$ is the force acting on atom i. In addition, we assume that the contribution ratios $p_{i,U_n^{(i)}}$ are independent of time and the local environment. Then, the time derivative of the atomic energy can be expressed as

$$\frac{d\varepsilon_i}{dt} = \sum_{\phi_n\in\mathscr{V}}\sum_{U_n^{(i)}\in\mathbf{U}_n}\sum_{j\in U_n^{(i)}}\left(p_{i,U_n^{(i)}}\mathbf{v}_j\cdot\mathbf{F}_j^{U_n^{(i)}} - p_{j,U_n^{(i)}}\mathbf{v}_i\cdot\mathbf{F}_i^{U_n^{(i)}}\right), \tag{19}$$

where $\mathbf{F}_i^{U_n^{(i)}}$ is $\partial\phi_n\left(U_n^{(i)}\right)/\partial\mathbf{r}_i$. We, thus, obtain the Torii formula,

$$V\mathbf{J}_{\mathrm{virial}}^{\mathrm{T}} = \sum_{i=1}^{N}\sum_{\phi_n\in\mathscr{V}}\sum_{U_n^{(i)}\in\mathbf{U}_n}\sum_{j\in U_n^{(i)}}\left(p_{i,U_n^{(i)}}\mathbf{v}_j\cdot\mathbf{F}_j^{U_n^{(i)}} - p_{j,U_n^{(i)}}\mathbf{v}_i\cdot\mathbf{F}_i^{U_n^{(i)}}\right)\mathbf{r}_i. \tag{20}$$

Our presentation of the Torii formula is different that what appears in Ref. 6 because we sum over the atomic clusters instead of over atomic indices. If we assume the energy equipartition $p_{i,U_n^{(i)}} = 1/n$, we get Surblys' centroid formula,

$$V\mathbf{J}_{\mathrm{virial}}^{\mathrm{C}} = -\sum_{i=1}^{N}\sum_{\phi_n\in\mathscr{V}}\sum_{U_n^{(i)}\in\mathbf{U}_n}\mathbf{v}_i\cdot\mathbf{F}_i^{U_n^{(i)}}\left(\mathbf{r}_i - \mathbf{r}_0^{U_n^{(i)}}\right). \tag{21}$$

Here, $\mathbf{r}_0^{U_n^{(i)}}$ is the center of mass of the atomic cluster $U_n^{(i)}$. A more detailed derivation of the Torii formula is provided in Sec. S1 of the supplementary material.

C. Fan formula

Langer *et al.*[46] previously demonstrated the applicability of the Fan formula to machine learning potentials. Further details are provided in Sec. S2 of the supplementary material. Using our notation, the Fan formula is

$$V\mathbf{J}_{\mathrm{virial}}^{\mathrm{F}} = \sum_{i=1}^{N}\sum_{j\in U(\mathfrak{n}_i)}\left(\mathbf{r}_{ij}\otimes\frac{\partial\psi_j}{\partial\mathbf{r}_i}\right)\mathbf{v}_i. \tag{22}$$

We define $\mathbf{r}_{ij}$ as $\mathbf{r}_j - \mathbf{r}_i$ and $U(\mathfrak{n}_i)$ as the set of atoms situated within a specific cutoff distance from atom i; this set will be discussed later. By assuming that the potential energy function is given by Eq. (3), we obtain the same expression as that derived by Fan *et al.*[37]

D. Equivalence between the Torii and Fan formulas

We now demonstrate the equivalence between the Torii and Fan formulas, which has not previously been shown. The first step is to define the potential functions and many-body atomic clusters with regard to the machine learning potential. In Sec. III B, although we considered the set of potential functions $\mathscr{V}$, a machine learning potential has only one composite function, represented as $\mathscr{V} = \{f^{\mathrm{ML}}\circ\phi\}$. Furthermore, the many-body atomic clusters can be expressed by the atomic indices in the LCE so that a set of atomic clusters can be represented as $\mathbf{U} = \{U(\mathfrak{n}_1), \ldots, U(\mathfrak{n}_N)\}$, where $U(\mathfrak{n}_i) = \{\, j \mid |\mathbf{r}_{ij}| \le R_c\}$ and R_c is the cutoff radius. Therefore, if $\mathscr{V}$ and $\mathbf{U}$ are substituted into the Torii formula, the

heat flux can be expressed as

$$V\mathbf{J}^{\mathrm{T}}_{\mathrm{virial}} = \sum_{i=1}^{N} \sum_{j=1, i\in U(\mathfrak{n}_j)}^{N} \sum_{k\in U(\mathfrak{n}_j)} \left(p_{i,U(\mathfrak{n}_j)} \mathbf{v}_k \cdot \mathbf{F}_k^{U(\mathfrak{n}_j)} - p_{k,U(\mathfrak{n}_j)} \mathbf{v}_i \cdot \mathbf{F}_i^{U(\mathfrak{n}_j)} \right) \mathbf{r}_i, \tag{23}$$

where $\mathbf{F}_i^{U(\mathfrak{n}_j)}$ is $\partial f^{\mathrm{ML}} \circ \boldsymbol{\phi}(\mathbf{r}_{\mathfrak{n}_j}) / \partial \mathbf{r}_i = \partial \boldsymbol{\psi}_j / \partial \mathbf{r}_i$. Assuming the same cutoff radius R_c for all atom pairs, then j satisfies $j \in U(\mathfrak{n}_i)$ if $i \in U(\mathfrak{n}_j)$. Therefore, we obtain

$$V\mathbf{J}^{\mathrm{T}}_{\mathrm{virial}} = \sum_{i=1}^{N} \sum_{j\in U(\mathfrak{n}_i)} \sum_{k\in U(\mathfrak{n}_j)} \left(p_{i,U(\mathfrak{n}_j)} \mathbf{v}_k \cdot \mathbf{F}_k^{U(\mathfrak{n}_j)} - p_{k,U(\mathfrak{n}_j)} \mathbf{v}_i \cdot \mathbf{F}_i^{U(\mathfrak{n}_j)} \right) \mathbf{r}_i. \tag{24}$$

We derived the centroid formula, Eq. (21), by assuming the equipartition of the interaction energy. However, the machine learning potential has only one potential function that directly calculates the atomic potential energy. Therefore, the contribution ratio for a machine learning potential is

$$p_{i,U(\mathfrak{n}_j)} = \delta_{i,j}, \tag{25}$$

where $\delta_{i,j}$ is the Kronecker delta. Thus, if the $p_{i,U(\mathfrak{n}_j)}$ are substituted into Eq. (24), we get

$$\begin{aligned} V\mathbf{J}^{\mathrm{T}}_{\mathrm{virial}} &= \sum_{i=1}^{N} \sum_{j\in U(\mathfrak{n}_i)} \sum_{k\in U(\mathfrak{n}_j)} \left(\delta_{i,j} \mathbf{v}_k \cdot \mathbf{F}_k^{U(\mathfrak{n}_j)} - \delta_{k,j} \mathbf{v}_i \cdot \mathbf{F}_i^{U(\mathfrak{n}_j)} \right) \mathbf{r}_i \\ &= \sum_{i=1}^{N} \sum_{k\in U(\mathfrak{n}_i)} \left(\mathbf{v}_k \cdot \mathbf{F}_k^{U(\mathfrak{n}_i)} \right) \mathbf{r}_i - \sum_{i=1}^{N} \sum_{j\in U(\mathfrak{n}_i)} \left(\mathbf{v}_i \cdot \mathbf{F}_i^{U(\mathfrak{n}_j)} \right) \mathbf{r}_i \\ &= \sum_{i=1}^{N} \sum_{j\in U(\mathfrak{n}_i)} \left(\mathbf{r}_{ij} \otimes \frac{\partial \psi_j}{\partial \mathbf{r}_i} \right) \mathbf{v}_i, \end{aligned} \tag{26}$$

and the final expression matches the Fan formula. A more detailed derivation is provided in Sec. S3 of the supplementary material.

Although we have limited ourselves here to the case of machine learning potentials, the same derivation is applicable to empirical potentials if we appropriately choose the potential functions and atomic clusters. For example, for the LJ potential, if we define the set of potential functions as $\mathscr{V} = \left\{ \sum_j \mathrm{LJ}(r_{ij})/2 \right\}$ and the set of atomic clusters as $\mathbf{U} = \{U(\mathfrak{n}_1), \ldots, U(\mathfrak{n}_N)\}$, we can derive the Fan formula in the same manner. Therefore, if we consider the equipartition of the interaction energies, such as in the centroid formula, and treat each as an energy function for the individual atoms, a derivation comparable to that for machine learning potentials is applicable.

It is important to note that the centroid formula cannot be applied to machine learning potentials because the assumption of equipartition does not hold. The Torii formula or the Fan formula should be used, with the choice as an implementation decision.

IV. RESULTS

A. MD simulations

We now investigate the difference between the accurate heat flux formula presented earlier [Eq. (26)] and the default heat flux formula implemented in LAMMPS. We calculate the thermal conductivity using the Green–Kubo method [Eq. (1)]. Considering the gauge invariance of the heat flux has recently been shown to be important under some conditions.[39,52] Because we only model single elements substances (silicon and copper), a renormalized heat flux is not required. Furthermore, we limit our analysis to a comparison of the thermal conductivity from the virial term contribution to the heat flux because the formulation of the convective term is unambiguous.

We selected silicon and copper because of their different bonding characteristics and because open-source potentials are available[21,53] for both the Spectral Neighbor Analysis Potential (SNAP)[16] and Atomic Cluster Expansion machine learning potential (PACE).[20,21] We also independently trained an MTP machine learning potential for each material, with details provided in the Appendix.[19] These three machine learning potentials all have a LAMMPS interface.

For silicon, the supercell size was $5 \times 5 \times 5$ (1000 atoms), the time step was 1 fs, the atomic mass is taken as 28.085 amu, and periodic boundary conditions were applied in all directions. The system was equilibrated for 1 ns via *NPT* simulation with a damping parameter of 1 ps. *NVE* simulation was performed for 1 ns of equilibration, followed by 6 ns for the heat flux data collection. A correlation time of 300 ps was used to calculate the autocorrelation of the heat flux. For copper, where we are only investigating the lattice thermal conductivity, a supercell size of $5 \times 5 \times 5$ (500 atoms) was used with a time step of 1 fs and an atomic mass of 63.546 amu. The system was equilibrated for 1 ns via *NPT* simulation with a damping parameter of 1 ps. The system was then equilibrated in an *NVE* simulation for 1 ns, followed by 3 ns for the heat flux data collection. We used a correlation time of 150 ps to calculate the autocorrelation of the heat flux. For each simulation, the heat flux was calculated using the accurate formula presented here and using the default LAMMPS implementation.

LAMMPS implements the heat flux for SNAP and PACE as

$$V\mathbf{J}^{\mathrm{LAMMPS}}_{\mathrm{virial}} = -\sum_{i=1}^{N} \sigma_i^{\mathrm{LAMMPS}} \mathbf{v}_i, \tag{27}$$

$$\sigma_i^{\mathrm{LAMMPS}} = \sum_{j\neq i} \mathbf{r}_{ji} \otimes \frac{\partial}{\partial \mathbf{r}_{ji}} \left\{ \frac{1}{2} \left(\psi_i + \psi_j \right) \right\}. \tag{28}$$

The heat flux in Eq. (27) is strictly accurate for two-body interatomic potentials. It is not accurate, however, for SNAP and PACE because the assumption that $\partial \psi_i / \partial \mathbf{r}_{ji} = \partial \psi_j / \partial \mathbf{r}_{ji}$ is not satisfied for many-body interactions. We implemented a function to compute the per-atomic stress tensors for the machine learning potentials in LAMMPS and used it to calculate the heat flux.

The MLIP package used to train the MTP has a LAMMPS interface and per-atomic stress tensors are implemented inside it.[19]

The implemented formula is

$$V\mathbf{J}^{\mathrm{MTP}}_{\mathrm{virial}} = -\sum_{i=1}^{N} \sigma_i^{\mathrm{MTP}} \mathbf{v}_i, \tag{29}$$

$$\sigma_i^{\mathrm{MTP}} = \sum_{j \neq i} \mathbf{r}_{ji} \otimes \frac{\partial \psi_i}{\partial \mathbf{r}_{ji}}. \tag{30}$$

This formula is also accurate for two-body potentials. It is not accurate, however, for a general MTP because the assumption that $\partial\psi_i/\partial\mathbf{r}_{ji} = \partial\psi_j/\partial\mathbf{r}_{ji}$ is not satisfied for many-body interactions. Tai *et al.* recently reported a discrepancy between the Fan formula for MTP and its implementation in LAMMPS.[54] While their work is focused on the Fan formula and MTP, our study addresses this issue for the Torii formula and general MLPs.

The results at a temperature of 300 K and zero pressure are shown in Figs. 1(a)–1(f). Each sub-figure shows the thermal conductivity from Eq. (1) plotted vs the correlation time, which is set as the upper limit of the Green–Kubo integral. Because silicon and copper are cubically isotropic, the results for the *x*-, *y*-, and *z*-directions are averaged. Further averaging is performed over five independent velocity seeds. The solid curves represent the mean thermal conductivity and the shaded regions represent the associated standard deviation. The label "Accurate" represents the thermal conductivity calculated using Eq. (26) for the heat flux and "LAMMPS" represents the thermal conductivity calculated by using Eqs. (27) or (29).

Because the "Accurate" and "LAMMPS" thermal conductivities are calculated from the same atomic trajectories, equivalent results would be expected if the default LAMMPS heat flux implementation was accurate. There are, however, discrepancies for both materials and all three potentials. To evaluate this difference, we define the error as $|\kappa_A - \kappa_D| \times 100/\kappa_A(\%)$, where κ_A is the accurate thermal conductivity calculated using Eq. (26) and κ_D is the default thermal conductivity according to Eqs. (27) or (29). We defined the converged thermal conductivity as the average over the final 50 ps of the correlation. These errors are provided in Table I, with values ranging from $-25\%$to$+22\%$. The sign $+/-$ indicates the over- or underestimation of the calculated thermal conductivity by the default LAMMPS implementation compared to the accurate implementation. There is no systematic trend, which suggests a complex interplay between the effects of the machine learning potential and the chemical composition/structure.

B. Comparison to BTE calculations

To validate the heat flux equation given by Eq. (26), the copper SNAP EMD thermal conductivities are compared to those calculated using the BTE. Under the relaxation time approximation (RTA), thermal conductivity can be expressed as

$$\kappa = \frac{1}{VN_{\mathbf{k}}} \sum_{s,\mathbf{k}} \hbar\omega_{s,\mathbf{k}} (\mathbf{v}_{s,\mathbf{k}} \otimes \mathbf{v}_{s,\mathbf{k}}) \tau_{s,\mathbf{k}} \frac{\partial f_{\mathrm{BE}(\omega_{s,\mathbf{k}},T)}}{\partial T}. \tag{31}$$

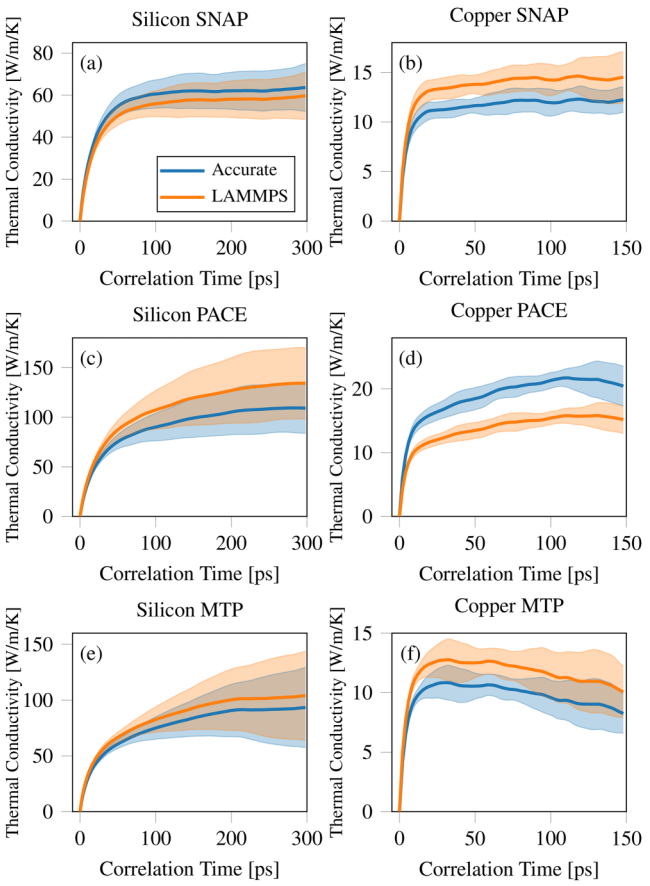

FIG. 1. Comparison of different implementations of the heat flux for silicon [(a), (c), and (e)] and copper [(b), (d), and (f)] using the SNAP [(a) anf (b)], ACE [(c) and (d)], and MTP [(e) and (f)] machine learning potentials. "LAMMPS" represents the thermal conductivity calculated by the default LAMMPS heat flux formula [Eqs. (27) or (29)] and "Accurate" represents the thermal conductivity calculated by the accurate heat flux formula [Eq. (26)]. The temperature is 300 K and the pressure is 0 bar.

In Eq. (31), s is the phonon branch, $\mathbf{k}$ is the wave vector, $N_{\mathbf{k}}$ is the number of wave vectors, $\omega_{s,\mathbf{k}}$ is the phonon frequency, $f_{\mathrm{BE}}(\omega_{s,\mathbf{k}}, T)$ is the Bose–Einstein distribution, $\mathbf{v}_{s,\mathbf{k}}$ is the group velocity, and $\tau_{s,\mathbf{k}}$ is the relaxation time.

TABLE I. Error (%) of thermal conductivity between the accurate formula [Eq. (26)] and the default LAMMPS implementation [Eqs. (27) or (29)]. The sign +/ − indicates over- or underestimation of the calculated thermal conductivity by the default LAMMPS implementation.

	Silicon	Copper
SNAP	6.4(−)	19(+)
PACE	22(+)	26(−)
MTP	11(+)	21(+)

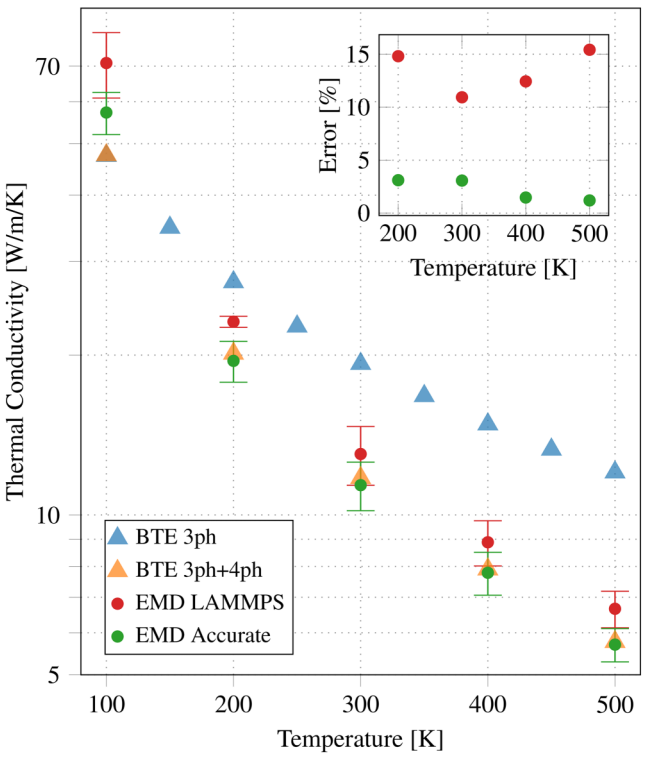

FIG. 2. Temperature-dependent thermal conductivity of copper with SNAP, comparing the EMD results with BTE. The accurate implementation of the heat flux gives values close to BTE 3ph+4ph. The inset shows the percentage error in thermal conductivity between EMD and BTE 3ph+4ph.

We used ALAMODE[55] to calculate the interatomic force constants (IFCs) and FourPhonon[56–59] to calculate the thermal conductivity. For calculating the IFCs, the system is an $8 \times 8 \times 8$ supercell of the primitive unit cell. The displacements for the second-, third-, and fourth-order IFCs are 0.01, 0.04, and 0.1 Å The cutoff radii for the second-, third-, and fourth-order IFCs are 5.8, 5.8, and 2.7 Å. The least-squares method was used to calculate the IFCs. In the thermal conductivity calculation, three- and four-phonon scatterings were considered. Phonon-isotope scattering is not included. The scale parameter for the Gaussian smearing that approximates the delta function for energy conversion in the phonon interactions (i.e., *scalebroad*) was 1.0. We used an iterative method for the three-phonon scattering and the RTA method for the four-phonon scattering. The relaxation time spectrum at a temperature of 300 K is shown in Sec. S4 of the supplementary material. We used **k**-point meshes of $40 \times 40 \times 40$ for the thermal conductivity calculated considering only three-phonon scattering (BTE 3ph) and $23 \times 23 \times 23$ for the thermal conductivity calculated considering three- and four-phonon scatterings (BTE 3ph+4ph). The relaxation time for each phonon mode was evaluated by the random sampling of 10^5 scattering processes from all scattering processes.[59]

The temperature-dependent thermal conductivities are plotted in Fig. 2 and the corresponding data are presented in Table II. For BTE 3ph+4ph, the calculations were repeated five times using the random sampling method and then averaged. Their standard deviations were at most 0.03 W/m/K; therefore, error bars are not shown in Fig. 2. The EMD results were calculated using the method described in Sec. IV A. The EMD points in Fig. 2 represent the averaged thermal conductivity over ten trajectories and the error bars denote the standard deviations. As shown in Sec. S5 of the supplementary material, the EMD results are converged with the size of the simulation cell.

Both sets of EMD results exhibit a temperature dependence similar to that of BTE 3ph+4ph, pointing to the importance of including four-phonon scattering as temperature is increased. The results using the accurate heat flux formula ($\kappa_{\mathrm{EMD}}^{\mathrm{Accurate}}$) agree well with BTE 3ph+4ph (κ_{BTE}) compared to the results using the default formula ($\kappa_{\mathrm{EMD}}^{\mathrm{LAMMPS}}$). The inset illustrates the percentage error in thermal conductivity between EMD and BTE, expressed as $|\kappa_{\mathrm{EMD}} - \kappa_{\mathrm{BTE}}| \times 100/\kappa_{\mathrm{BTE}}$ (%). The larger differences at a temperature of 100 K can be attributed to the classical statistics and finite sampling time effects in the EMD simulations. To evaluate the effect of the statistics, we also calculated thermal conductivity using BTE-RTA and classical statistics with only three-phonon scattering. The ratio of the classical thermal conductivity to the quantum thermal conductivity is 1.10 at a temperature of 100 K and is below 1.02 at temperatures of 300 K and higher temperatures. Therefore, it can be concluded that the overestimate at 100 K is due to the quantum effect. Moreover, quantum effects at 300 K and above can be ignored. Furthermore, we performed the BTE calculations and EMD simulations for MTP and PACE for copper at 300 K. The EMD results are lower than the BTE 3ph+4ph results, as opposed to the agreement found for SNAP. The discrepancy can be attributed to fifth-order and higher phonon scattering. SNAP, by its functional form, is limited to a maximum of four-body interactions. Consequently, its fifth-order and higher interatomic force constants are identically zero, meaning all phonon scattering is described by processes up to the fourth order. MTP and PACE, on the other hand, incorporate many-body interactions beyond the fourth order.

TABLE II. Thermal conductivity (W/m/K) comparison of BTE and EMD. All calculations are performed for copper, with SNAP at 200–500 K, and MTP and PACE at 300 K only.

	200 (K)	300 (K)	400 (K)	500 (K)	300 (K) for MTP	300 (K) for PACE
BTE 3ph	27.4	19.3	14.8	12.0	20.9	25.2
BTE 3ph+4ph	20.1	11.7	7.90	5.77	15.9	19.8
EMD Accurate	19.5 ± 1.7	11.4 ± 1.2	7.78 ± 0.72	5.70 ± 0.41	7.87 ± 0.83	15.5 ± 1.85
EMD LAMMPS	23.1 ± 0.6	13.0 ± 1.7	8.88 ± 0.87	6.66 ± 0.53	9.91 ± 0.80	10.1 ± 0.86

V. SUMMARY

To generalize the use of the Green–Kubo method for calculating thermal conductivity in an EMD simulation, we derived a form of the Torii heat flux formula that is applicable to machine learning potentials [Eq. (26)]. This heat flux formula was validated using a test case of Cu modeled with a SNAP potential. The Green–Kubo predicted thermal conductivities showed good agreement with calculations performed using lattice dynamics calculations and the BTE (Fig. 2 and Table II). We also demonstrated the equivalence of the Torii and Fan heat flux formulas for both empirical and machine learning potentials (Sec. III D). Our recommendation is to use the centroid formula [Eq. (21)] for empirical potentials that use energy equipartition and the Fan formula [Eqs. (22) and (26)] for other potentials, including machine learning potentials. This recommendation is based on the fact that machine learning potentials do not satisfy the equipartition condition and the centroid formula is generally less computationally expensive than the Fan formula.

To assess the impact of the selection of the heat flux formula, we performed EMD simulations of Si and Cu using three different machine learning potentials (SNAP, ACE, and MTP) and calculated the thermal conductivity using the Green–Kubo method. As shown in Fig. 1 and Table I, the heat flux formula implemented in LAMMPS can overestimate or underestimate the thermal conductivity obtained from the accurate formula, with no trend across potentials or materials. This finding points to the caution that should be taken when calculating the heat flux. It is important to ensure that the formula implemented in a given package is consistent with the form of empirical potential or a machine learning potential used to describe the atomic interactions.

SUPPLEMENTARY MATERIAL

See the supplementary material for information about the detailed derivation of the Torii formula and the Fan formula, the size effect analysis of the Green–Kubo approach for copper, and the third and fourth-order relaxation time spectrum for copper.

ACKNOWLEDGMENTS

This study was financially supported in part by KAKENHI (Grant No. 22H04950) from the Japan Society for the Promotion of Science (JSPS) and CREST (Grant No. JPMJCR21O2) provided by the Japan Science and Technology Agency (JST). T.H. was supported by the Quantum Science and Technology Fellowship Program (Q-STEP) and a Research Fellowship for Young Scientists DC2 (Grant No. 23KJ0511) from JSPS. A.J.H.M. was supported by Army Research Office through Award No. W911NF2220191.

AUTHOR DECLARATIONS

Conflict of Interest

The authors have no conflicts to disclose.

Author Contributions

Tomu Hamakawa: Conceptualization (equal); Data curation (lead); Formal analysis (lead); Investigation (lead); Methodology (lead); Validation (lead); Writing – original draft (lead). **Alan J. H. McGaughey:** Investigation (equal); Methodology (equal); Supervision (equal); Writing – review & editing (equal). **Junichiro Shiomi:** Conceptualization (equal); Funding acquisition (equal); Project administration (equal); Resources (equal); Supervision (equal); Writing – review & editing (equal).

DATA AVAILABILITY

The implementation and trained potentials are publically available in GitHub at https://github.com/tomuhama/HeatFlux_MLP_LAMMPS, Ref. 71.

APPENDIX: MTP TRAINING DETAIL

We used the MLIP-2 package and adopted active learning.[19] The selection threshold for active learning is 1.8, and the cutoff radii are $R_{\min} = 1.9$ Å and $R_{\max} = 6.0$ Å. We performed several *ab initio NPT* MD simulations for active learning until no training data were added. In addition, we used $(w_e, w_f, w_s) = (1, 0.1, 0.01)$ for the weights of energy, force, and stress during training.[51]

We used VASP 5.4 for the silicon training data.[60–63] The DFT calculation conditions were as follows: a supercell of $3 \times 3 \times 3$ (216 atoms), the PAW method,[64] the GGA-PBE functional,[65,66] VASP POTCAR file ver. 5 January 2001 for the pseudopotential, 650 eV energy cutoff for plane waves, adopting the second-order Methfessel–Paxton method,[67] 0.05 eV for the smearing width, 10^{-8} eV for the threshold of the calculation, and a $6 \times 6 \times 6$ Γ-centered **q**-point mesh. For the training data at 300 K, the mean absolute error (MAE) was 0.23 meV/atom for the per-atom energy, 7.40 meV/Å for the forces, and 5.39×10^{-3} GPa for the stresses.

We used Quantum ESPRESSO[68,69] v6.8 for the copper training data. The DFT calculation conditions are as follows: a supercell of $2 \times 2 \times 2$(64 atoms), the PAW method,[64] the GGA-PBEsol functional,[70] the pslibrary for pseudopotential (Cu.pbesol-dn-kjpaw_psl.1.0.0), 816.34 eV (60 Ry) energy cutoff for plane waves, adopting the first-order Methfessel–Paxton method,[67] 0.068 eV (0.005 Ry) for the smearing width, 10^{-8} Ry for the threshold of the SCF calculation, and a $4 \times 4 \times 4$ Γ-centered **q**-point mesh. For the training data at 1000 K, the MAE was 2.87 meV/atom for the per-atom energy and 45.0 meV/Å for forces. The potential for copper was trained only on the energies and forces, as preliminary tests revealed that the inclusion of stress data degraded the model's predictive accuracy.

REFERENCES

[1]E. Pop, S. Sinha, and K. Goodson, "Heat generation and transport in nanometer-scale transistors," Proc. IEEE **94**, 1587–1601 (2006).
[2]H. J. Goldsmid, *Introduction to Thermoelectricity*, Springer Series in Materials Science Vol. 121 (Springer, Berlin, 2016).
[3]A. S. Henry and G. Chen, "Spectral phonon transport properties of silicon based on molecular dynamics simulations and lattice dynamics," J. Comput. Theor. Nanosci. **5**, 141–152 (2008).
[4]J. A. Thomas, J. E. Turney, R. M. Iutzi, C. H. Amon, and A. J. H. McGaughey, "Predicting phonon dispersion relations and lifetimes from the spectral energy density," Phys. Rev. B **81**, 081411 (2010).
[5]K. Esfarjani, G. Chen, and H. T. Stokes, "Heat transport in silicon from first-principles calculations," Phys. Rev. B **84**, 085204 (2011).

[6]D. Torii, T. Nakano, and T. Ohara, "Contribution of inter- and intramolecular energy transfers to heat conduction in liquids," J. Chem. Phys. **128**, 044504 (2008).
[7]A. J. H. McGaughey, A. Jain, H.-Y. Kim, and B. Fu, "Phonon properties and thermal conductivity from first principles, lattice dynamics, and the Boltzmann transport equation," J. Appl. Phys. **125**, 011101 (2019).
[8]X. Gu, Z. Fan, and H. Bao, "Thermal conductivity prediction by atomistic simulation methods: Recent advances and detailed comparison," J. Appl. Phys. **130**, 210902 (2021).
[9]D. A. Broido, A. Ward, and N. Mingo, "Lattice thermal conductivity of silicon from empirical interatomic potentials," Phys. Rev. B **72**, 014308 (2005).
[10]A. Ward, D. A. Broido, D. A. Stewart, and G. Deinzer, "*Ab initio* theory of the lattice thermal conductivity in diamond," Phys. Rev. B **80**, 125203 (2009).
[11]J. Behler and M. Parrinello, "Generalized neural-network representation of high-dimensional potential-energy surfaces," Phys. Rev. Lett. **98**, 146401 (2007).
[12]A. P. Bartók, M. C. Payne, R. Kondor, and G. Csányi, "Gaussian approximation potentials: The accuracy of quantum mechanics, without the electrons," Phys. Rev. Lett. **104**, 136403 (2010).
[13]M. A. Caro, "Optimizing many-body atomic descriptors for enhanced computational performance of machine learning based interatomic potentials," Phys. Rev. B **100**, 024112 (2019).
[14]J. Byggmästar, K. Nordlund, and F. Djurabekova, "Simple machine-learned interatomic potentials for complex alloys," Phys. Rev. Mater. **6**, 083801 (2022).
[15]H. Wang, L. Zhang, J. Han, and W. E, "DeePMD-kit: A deep learning package for many-body potential energy representation and molecular dynamics," Comput. Phys. Commun. **228**, 178–184 (2018).
[16]A. Thompson, L. Swiler, C. Trott, S. Foiles, and G. Tucker, "Spectral neighbor analysis method for automated generation of quantum-accurate interatomic potentials," J. Comput. Phys. **285**, 316–330 (2015).
[17]M. A. Wood and A. P. Thompson, "Extending the accuracy of the SNAP interatomic potential form," J. Chem. Phys. **148**, 241721 (2018).
[18]A. V. Shapeev, "Moment tensor potentials: A class of systematically improvable interatomic potentials," Multiscale Model. Simul. **14**, 1153–1173 (2016).
[19]I. S. Novikov, K. Gubaev, E. V. Podryabinkin, and A. V. Shapeev, "The MLIP package: Moment tensor potentials with MPI and active learning," Mach. Learn. Sci. Technol. **2**, 025002 (2021).
[20]R. Drautz, "Atomic cluster expansion for accurate and transferable interatomic potentials," Phys. Rev. B **99**, 014104 (2019).
[21]Y. Lysogorskiy, C. V. D. Oord, A. Bochkarev, S. Menon, M. Rinaldi, T. Hammerschmidt, M. Mrovec, A. Thompson, G. Csányi, C. Ortner, and R. Drautz, "Performant implementation of the atomic cluster expansion (PACE) and application to copper and silicon," npj Comput. Mater. **7**, 97 (2021).
[22]Z. Fan, Z. Zeng, C. Zhang, Y. Wang, K. Song, H. Dong, Y. Chen, and T. Ala-Nissila, "Neuroevolution machine learning potentials: Combining high accuracy and low cost in atomistic simulations and application to heat transport," Phys. Rev. B **104**, 104309 (2021).
[23]Z. Fan, "Improving the accuracy of the neuroevolution machine learning potential for multi-component systems," J. Phys.: Condens. Matter **34**, 125902 (2022).
[24]S. Batzner, A. Musaelian, L. Sun, M. Geiger, J. P. Mailoa, M. Kornbluth, N. Molinari, T. E. Smidt, and B. Kozinsky, "E(3)-equivariant graph neural networks for data-efficient and accurate interatomic potentials," Nat. Commun. **13**, 2453 (2022).
[25]F. Müller-Plathe, "A simple nonequilibrium molecular dynamics method for calculating the thermal conductivity," J. Chem. Phys. **106**, 6082–6085 (1997).
[26]R. Kubo, M. Yokota, and S. Nakajima, "Statistical-mechanical theory of irreversible processes. II. Response to thermal disturbance," J. Phys. Soc. Jpn. **12**, 1203–1211 (1957).
[27]J. H. Irving and J. G. Kirkwood, "The statistical mechanical theory of transport processes. IV. The equations of hydrodynamics," J. Chem. Phys. **18**, 817–829 (1950).
[28]E. Helfand, "Transport coefficients from dissipation in a canonical ensemble," Phys. Rev. **119**, 1–9 (1960).
[29]D. A. McQuarrie, *Statistical Mechanics* (Harper & Row, 1975).
[30]R. J. Hardy, "Energy-flux operator for a lattice," Phys. Rev. **132**, 168–177 (1963).
[31]T. Ohara, T. Chia Yuan, D. Torii, G. Kikugawa, and N. Kosugi, "Heat conduction in chain polymer liquids: Molecular dynamics study on the contributions of inter- and intramolecular energy transfer," J. Chem. Phys. **135**, 034507 (2011).
[32]D. Surblys, H. Matsubara, G. Kikugawa, and T. Ohara, "Application of atomic stress to compute heat flux via molecular dynamics for systems with many-body interactions," Phys. Rev. E **99**, 051301 (2019).
[33]D. Surblys, H. Matsubara, G. Kikugawa, and T. Ohara, "Methodology and meaning of computing heat flux via atomic stress in systems with constraint dynamics," J. Appl. Phys. **130**, 215104 (2021).
[34]A. P. Thompson, H. M. Aktulga, R. Berger, D. S. Bolintineanu, W. M. Brown, P. S. Crozier, P. J. In 'T Veld, A. Kohlmeyer, S. G. Moore, T. D. Nguyen, R. Shan, M. J. Stevens, J. Tranchida, C. Trott, and S. J. Plimpton, "LAMMPS—A flexible simulation tool for particle-based materials modeling at the atomic, meso, and continuum scales," Comput. Phys. Commun. **271**, 108171 (2022).
[35]A. P. Thompson, S. J. Plimpton, and W. Mattson, "General formulation of pressure and stress tensor for arbitrary many-body interaction potentials under periodic boundary conditions," J. Chem. Phys. **131**, 154107 (2009).
[36]P. Boone, H. Babaei, and C. E. Wilmer, "Heat flux for many-body interactions: Corrections to LAMMPS," J. Chem. Theory Comput. **15**, 5579–5587 (2019).
[37]Z. Fan, L. F. C. Pereira, H.-Q. Wang, J.-C. Zheng, D. Donadio, and A. Harju, "Force and heat current formulas for many-body potentials in molecular dynamics simulations with applications to thermal conductivity calculations," Phys. Rev. B **92**, 094301 (2015).
[38]Z. Fan, Y. Wang, P. Ying, K. Song, J. Wang, Y. Wang, Z. Zeng, K. Xu, E. Lindgren, J. M. Rahm, A. J. Gabourie, J. Liu, H. Dong, J. Wu, Y. Chen, Z. Zhong, J. Sun, P. Erhart, Y. Su, and T. Ala-Nissila, "GPUMD: A package for constructing accurate machine-learned potentials and performing highly efficient atomistic simulations," J. Chem. Phys. **157**, 114801 (2022).
[39]A. Marcolongo, L. Ercole, and S. Baroni, "Gauge fixing for heat-transport simulations," J. Chem. Theory Comput. **16**, 3352–3362 (2020).
[40]R. Bertossa, F. Grasselli, L. Ercole, and S. Baroni, "Theory and numerical simulation of heat transport in multicomponent systems," Phys. Rev. Lett. **122**, 255901 (2019).
[41]L. Ercole, A. Marcolongo, and S. Baroni, "Accurate thermal conductivities from optimally short molecular dynamics simulations," Sci. Rep. **7**, 15835 (2017).
[42]G. C. Sosso, D. Donadio, S. Caravati, J. Behler, and M. Bernasconi, "Thermal transport in phase-change materials from atomistic simulations," Phys. Rev. B **86**, 104301 (2012).
[43]X. Gu and C. Zhao, "Thermal conductivity of single-layer $MoS_{2(1-x)}Se_{2x}$ alloys from molecular dynamics simulations with a machine-learning-based interatomic potential," Comput. Mater. Sci. **165**, 74–81 (2019).
[44]X. Qian, S. Peng, X. Li, Y. Wei, and R. Yang, "Thermal conductivity modeling using machine learning potentials: Application to crystalline and amorphous silicon," Mater. Today Phys. **10**, 100140 (2019).
[45]P. Korotaev, I. Novoselov, A. Yanilkin, and A. Shapeev, "Accessing thermal conductivity of complex compounds by machine learning interatomic potentials," Phys. Rev. B **100**, 144308 (2019).
[46]M. F. Langer, F. Knoop, C. Carbogno, M. Scheffler, and M. Rupp, "Heat flux for semilocal machine-learning potentials," Phys. Rev. B **108**, L100302 (2023).
[47]For multi-species systems, atomic energies are expressed as the sum of all interactions. For example, for a Si–Ge system, the total potential energy is a sum of the potential energies for all Si–Si, Si–Ge, and Ge–Ge pairs. The potential energy of a Si atom, ε_{Si}, is determined by its LCE ρ in the MTP formalism. For a Si–Ge system, this LCE is decomposed by species, meaning it is described by the configurations of surrounding Si atoms (ρ_{Si}) and Ge atoms (ρ_{Ge}). The potential energy of the particular Si atom is then given by the sum of contributions from these interactions. A key aspect of the MTP formalism is that while the functional form $\varepsilon(\rho, c)$ is the same for each species, the parameters (c_{Si-Si}, c_{Si-Ge}), which are trained, are specific to each interacting element pair. This relationship

can be expressed formally as $\varepsilon_{Si} = \varepsilon(\rho_{Si-Si}, c_{Si-Si}) + \varepsilon(\rho_{Si-Ge}, c_{Si-Ge})$. Our framework can be applied by using the Torii formula for each of these functions.
[48]Although the atomic potential energy should depend on the all relative position vectors $\{\mathbf{r}_2 - \mathbf{r}_1, \ldots, \mathbf{r}_N - \mathbf{r}_{N-1}\}$, most interatomic potentials use this function form.
[49]A. P. Bartók, R. Kondor, and G. Csányi, "On representing chemical environments," Phys. Rev. B **87**, 184115 (2013).
[50]E. V. Podryabinkin and A. V. Shapeev, "Active learning of linearly parametrized interatomic potentials," Comput. Mater. Sci. **140**, 171–180 (2017).
[51]I. Novoselov, A. Yanilkin, A. Shapeev, and E. Podryabinkin, "Moment tensor potentials as a promising tool to study diffusion processes," Comput. Mater. Sci. **164**, 46–56 (2019).
[52]L. Ercole, A. Marcolongo, P. Umari, and S. Baroni, "Gauge invariance of thermal transport coefficients," J. Low Temp. Phys. **185**, 79–86 (2016).
[53]Y. Zuo, C. Chen, X. Li, Z. Deng, Y. Chen, J. Behler, G. Csányi, A. V. Shapeev, A. P. Thompson, M. A. Wood, and S. P. Ong, "Performance and cost assessment of machine learning interatomic potentials," J. Phys. Chem. A **124**, 731–745 (2020).
[54]S. T. Tai, C. Wang, R. Cheng, and Y. Chen, "Revisiting many-body interaction heat current and thermal conductivity calculations using the moment tensor potential/lammps interface," J. Chem. Theory Comput. **21**, 3649–3657 (2025).
[55]T. Tadano, Y. Gohda, and S. Tsuneyuki, "Anharmonic force constants extracted from first-principles molecular dynamics: Applications to heat transfer simulations," J. Phys.: Condens. Matter **26**, 225402 (2014).
[56]T. Feng and X. Ruan, "Quantum mechanical prediction of four-phonon scattering rates and reduced thermal conductivity of solids," Phys. Rev. B **93**, 045202 (2016).
[57]T. Feng, L. Lindsay, and X. Ruan, "Four-phonon scattering significantly reduces intrinsic thermal conductivity of solids," Phys. Rev. B **96**, 161201 (2017).
[58]Z. Han, X. Yang, W. Li, T. Feng, and X. Ruan, "FourPhonon: An extension module to ShengBTE for computing four-phonon scattering rates and thermal conductivity," Comput. Phys. Commun. **270**, 108179 (2022).
[59]Z. Guo, Z. Han, D. Feng, G. Lin, and X. Ruan, "Sampling-accelerated prediction of phonon scattering rates for converged thermal conductivity and radiative properties," npj Comput. Mater. **10**, 31 (2024).
[60]G. Kresse and J. Hafner, "*Ab initio* molecular dynamics for liquid metals," Phys. Rev. B **47**, 558–561 (1993).
[61]G. Kresse and J. Hafner, "*Ab initio* molecular-dynamics simulation of the liquid-metal–amorphous-semiconductor transition in germanium," Phys. Rev. B **49**, 14251–14269 (1994).
[62]G. Kresse and J. Furthmüller, "Efficient iterative schemes for *ab initio* total-energy calculations using a plane-wave basis set," Phys. Rev. B **54**, 11169–11186 (1996).
[63]G. Kresse and J. Furthmüller, "Efficiency of ab-initio total energy calculations for metals and semiconductors using a plane-wave basis set," Comput. Mater. Sci. **6**, 15–50 (1996).
[64]G. Kresse and D. Joubert, "From ultrasoft pseudopotentials to the projector augmented-wave method," Phys. Rev. B **59**, 1758–1775 (1999).
[65]J. P. Perdew, K. Burke, and M. Ernzerhof, "Generalized gradient approximation made simple," Phys. Rev. Lett. **77**, 3865–3868 (1996).
[66]J. P. Perdew, K. Burke, and M. Ernzerhof, "Generalized gradient approximation made simple [Phys. Rev. Lett. 77, 3865 (1996)]," Phys. Rev. Lett. **78**, 1396 (1997).
[67]M. Methfessel and A. T. Paxton, "High-precision sampling for Brillouin-zone integration in metals," Phys. Rev. B **40**, 3616–3621 (1989).
[68]P. Giannozzi, S. Baroni, N. Bonini, M. Calandra, R. Car, C. Cavazzoni, D. Ceresoli, G. L. Chiarotti, M. Cococcioni, I. Dabo, A. Dal Corso, S. De Gironcoli, S. Fabris, G. Fratesi, R. Gebauer, U. Gerstmann, C. Gougoussis, A. Kokalj, M. Lazzeri, L. Martin-Samos, N. Marzari, F. Mauri, R. Mazzarello, S. Paolini, A. Pasquarello, L. Paulatto, C. Sbraccia, S. Scandolo, G. Sclauzero, A. P. Seitsonen, A. Smogunov, P. Umari, and R. M. Wentzcovitch, "QUANTUM ESPRESSO: A modular and open-source software project for quantum simulations of materials," J. Phys.: Condens. Matter **21**, 395502 (2009).
[69]P. Giannozzi, O. Andreussi, T. Brumme, O. Bunau, M. Buongiorno Nardelli, M. Calandra, R. Car, C. Cavazzoni, D. Ceresoli, M. Cococcioni, N. Colonna, I. Carnimeo, A. Dal Corso, S. De Gironcoli, P. Delugas, R. A. DiStasio, A. Ferretti, A. Floris, G. Fratesi, G. Fugallo, R. Gebauer, U. Gerstmann, F. Giustino, T. Gorni, J. Jia, M. Kawamura, H.-Y. Ko, A. Kokalj, E. Küçükbenli, M. Lazzeri, M. Marsili, N. Marzari, F. Mauri, N. L. Nguyen, H.-V. Nguyen, A. Otero-de-la Roza, L. Paulatto, S. Poncé, D. Rocca, R. Sabatini, B. Santra, M. Schlipf, A. P. Seitsonen, A. Smogunov, I. Timrov, T. Thonhauser, P. Umari, N. Vast, X. Wu, and S. Baroni, "Advanced capabilities for materials modelling with QUANTUM ESPRESSO," J. Phys.: Condens. Matter **29**, 465901 (2017).
[70]J. P. Perdew, A. Ruzsinszky, G. I. Csonka, O. A. Vydrov, G. E. Scuseria, L. A. Constantin, X. Zhou, and K. Burke, "Restoring the density-gradient expansion for exchange in solids and surfaces," Phys. Rev. Lett. **100**, 136406 (2008).
[71]T. Hamakawa, "HeatFlux_MLP_LAMMPS," GitHub repository (2025), available at https://github.com/tomuhama/HeatFlux_MLP_LAMMPS.